IEEE Access
Multidisciplinary ⋮ Rapid Review ⋮ Open Access Journal

Received 10 May 2023, accepted 24 May 2023, date of publication 29 May 2023, date of current version 6 June 2023.

Digital Object Identifier 10.1109/ACCESS.2023.3281074

RESEARCH ARTICLE

Transmission-Line Schematic for Harmonic-Controlled Bandpass Filters

JONGHEUN LEE[1], (Graduate Student Member, IEEE), MINHYUP SONG[2], (Member, IEEE), AND JUSEOP LEE[1], (Senior Member, IEEE)

[1]Department of Computer and Radio Communications Engineering, Korea University, Seoul 02841, South Korea
[2]Photonic/Wireless Devices Research Division, Electronics and Telecommunications Research Institute (ETRI), Daejeon 34129, South Korea

Corresponding author: Juseop Lee (juseoplee@gmail.com)

This work was supported by the Institute for Information and Communication Technology Promotion (IITP) grant funded by the Ministry of Science and ICT, South Korea, under Grant 2019-0-00008.

ABSTRACT This article presents a rigorous synthesis method of a transmission-line filter whose second passband can be placed at any multiple of the center frequency, in theory. Two coupled-line schematics for harmonic-controlled bandpass filters are derived from fundamental *LC* filter prototypes. Their design parameters are provided in closed-form expressions so filter dimensions can be acquired rigorously without relying on EM-simulation-based coupling tests. Three filters were designed and fabricated for verification purposes, and their measurement results exhibited excellent agreement with the theory.

INDEX TERMS Filter design, filter synthesis, transmission-line filters.

I. INTRODUCTION

USING the concept of stepped impedance and adding one or multiple stubs are the popular approaches to move the second resonant frequency of a resonator to a high frequency. Designs of filters and filter-based circuits with broad upper stopbands can be carried out by making use of the aforementioned techniques [1], [2], [3], [4], [5], [6], [7], [8], [9]. In general, designing them begins with formulating the resonators and moves on to executing coupling tests to attain the dimensions delivering the target coupling coefficients through simulations. Obviously, this takes a significant amount of time as simulations should be repeated over a wide frequency range and the resonators have more discontinuities due to the stepped impedance and loaded stubs.

This article presents an accurate circuit-theory approach for designing harmonic-controlled filters. A handful of such approaches were explored a couple of decades ago [10], [11], [12], and, no fully rigorous method to formulate a bandpass filter schematic has been reported up to date. Here, we discuss an accurate formulation of the simplest, to the best of our knowledge, schematic for harmonic-controlled bandpass filters, which has the noticeable merits listed below:

1) It is made of the cascade of two-port coupled-line sections derived based on rigorous circuit transformations.
2) All design parameters of the coupled lines (modal admittances and electrical lengths) can be expressed mathematically in terms of a target response.
3) It has only two types of two-port coupled-line sections, and those of the same type have the same length.
4) No discontinuity exists in each coupled-line section.
5) It has the same number of coupled-line sections as conventional coupled-line filters (n+1 coupled-line sections for an nth-order filter).

These merits allow us to find the initial dimensions of a harmonic-controlled filter structure without executing trial-and-error coupling tests, and this differentiates our approach and schematic from the others.

The associate editor coordinating the review of this manuscript and approving it for publication was Giorgio Montisci.

II. THEORY

A. STUBS (RESONATORS)

Various types of resonator structures are illustrated in Fig. 1. Those in the second column are recognized as *Richards-equivalent circuits* of lumped-element resonators, presented by P. I. Richards [13]. They are quarter-wavelength long, *i.e.*,

$$\theta_0 = \frac{\pi}{2} \ (= 90^\circ), \tag{1}$$

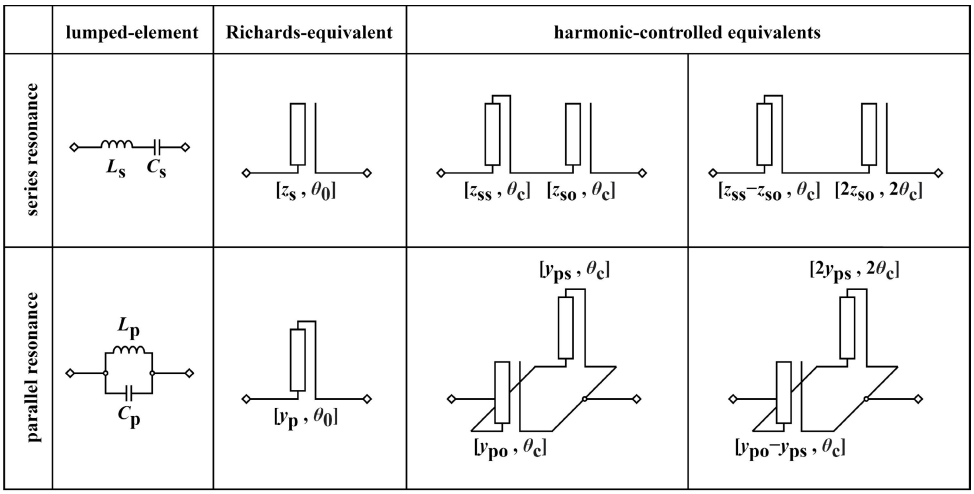

FIGURE 1. Summary of resonators.

at the first resonant frequency (f_0) of their lumped-element counterparts. The characteristic immittances (z_s and y_p) are determined such that each has the immittance slope (variation of immittance with respect to the frequency) identical to that of the corresponding LC pairs at f_0 as

$$z_s = 8f_0 L_s \tag{2a}$$
$$y_p = 8f_0 C_p. \tag{2b}$$

Equations (1) and (2) indicate that there exists no degree of freedom in determining the parameters of quarter-wavelength stubs when an LC pair is given. Hence, it is inevitable that the stubs periodically resonate at odd-multiples of f_0.

On the other hand, the stub structures in the third and the fourth columns of Fig. 1, referred to as harmonic-controlled equivalents, are capable of controlling the second resonant frequency, in addition to the immittance slope and the first resonant frequency. The design parameters of the stubs in the third column are found by imposing the following three conditions that

- The first resonance of each stub structure occurs at f_0.
- The second resonance of each stub structure occurs at mf_0 (m: any positive real number in theory).
- Each stub structure has the same immittance slope as the corresponding Richards-equivalent resonator at f_0,

which gives

$$\theta_c = \frac{\pi}{m+1} \tag{3}$$

at f_0 with (series resonators in the first row)

$$z_{ss} = z_s \cdot \frac{\pi}{4} \cdot \frac{(\cos\theta_c)^2}{\theta_c}$$
$$z_{so} = z_s \cdot \frac{\pi}{4} \cdot \frac{(\sin\theta_c)^2}{\theta_c}, \tag{4a}$$

and (parallel resonators in the second row)

$$y_{ps} = y_p \cdot \frac{\pi}{4} \cdot \frac{(\sin\theta_c)^2}{\theta_c}$$
$$y_{po} = y_p \cdot \frac{\pi}{4} \cdot \frac{(\cos\theta_c)^2}{\theta_c}. \tag{4b}$$

The stub structures in the fourth column are found by applying Podcameni's equivalent-circuit transformations [14] to those in the third column. The design parameters of these stubs are found by utilizing the identity as well.

B. FILTER SCHEMATIC

Fig. 2 shows the prototype circuit of an nth-order bandpass filter (n = even number) made of series-LC inductors and impedance inverters. This figure also shows the scheme for transforming the prototype circuit into a pure distributed-element circuit whose second passband can be placed at mf_0.

The series-LC resonators are implemented with the harmonic-controlled resonators shown in the first row-fourth column of Fig. 1. The inverters are implemented with two distinct inverter structures, and this was to further ease the manipulation of the series stubs comprising the harmonic-controlled resonators. Even though these inverter structures produce the phase shifts that are opposite to each other, it is of no significance as the circuit schematic does not consist of cross couplings (two or more sub-paths connected in parallel).

The first structure, used to implement the inverter, K_{12}, has three short-circuited stubs (T-type inductors). Each stub length can be arbitrarily chosen to some extent, but preferably shorter than one eighth ($\theta < 45°$) of the center-frequency wavelength. Considering that the series stubs can only be absorbed into those comprising the harmonic-controlled resonators when they are equal in length, it is suggested to let

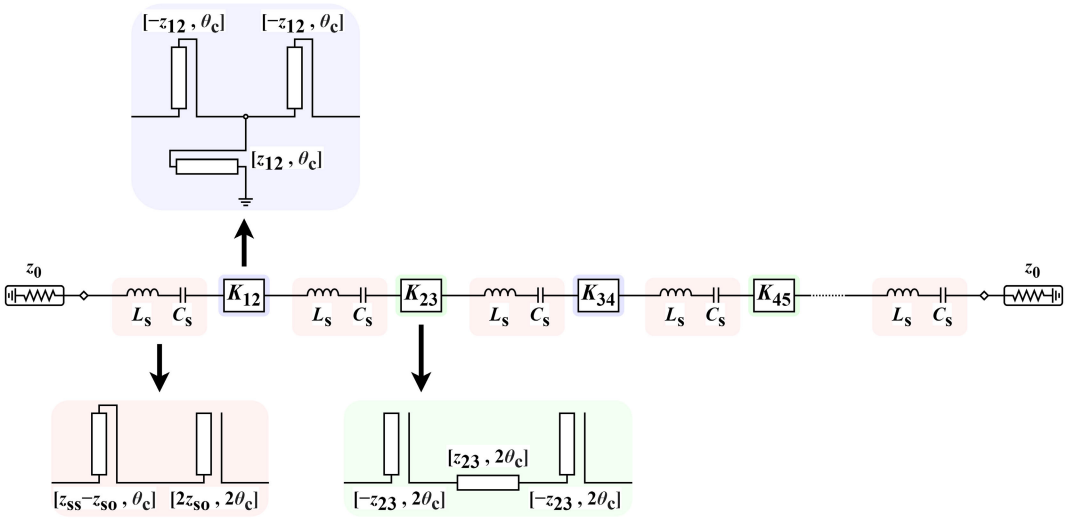

FIGURE 2. Bandpass prototype circuit and its transformation scheme.

TABLE 1. Parameter values of the designed sixth-order filter. Units for the impedance-parameter values are Ω.

θ_c	z_{ss}	z_{so}	z_{12} (=z_{56})	z_{23} (=z_{45})	z_{34}
15°	70.85	5.086	3.13	0.30385	2.16

them be θ_c long at f_0, providing the following equation of

$$z_{12} = |K_{12}| \cdot \cot\theta_c. \tag{5}$$

On the contrary, it is not preferred to implement the upcoming inverter (K_{23} in this case) with T-type stubs since it would be difficult to further manipulate the remaining open-circuited series stub (positioned between inverters K_{12} and K_{23}). For this reason, this work utilizes two negative-impedance stubs and a positive-impedance line section in between to implement the inverter, K_{23}. They should be $2\theta_c$ long at f_0 so that the negative-impedance open-circuited series stubs can be absorbed into the adjoining resonators. Their characteristic impedances are then

$$z_{23} = |K_{23}| \cdot \sin(2\theta_c). \tag{6}$$

The above-mentioned structures are alternately employed to implement the remaining inverters as indicated in Fig. 2.

For demonstration, a filter was designed to produce

- a sixth-order ($n = 6$) Chebyshev response with 20 dB-equi-ripple return loss;
- the fractional bandwidth of 0.05;
- the second passband centered at $11f_0$ ($m = 11$).

The parameter values were computed under the condition that $z_0 = 1\ \Omega$. The computed parameter values are summarized in Table 1. The response of this filter is plotted in Fig. 3. It is worth highlighting that the spurious-free stopband up to mf_0 in Fig. 3(a) can be secured only when the electrical lengths of the line components adhere to Fig. 2. One

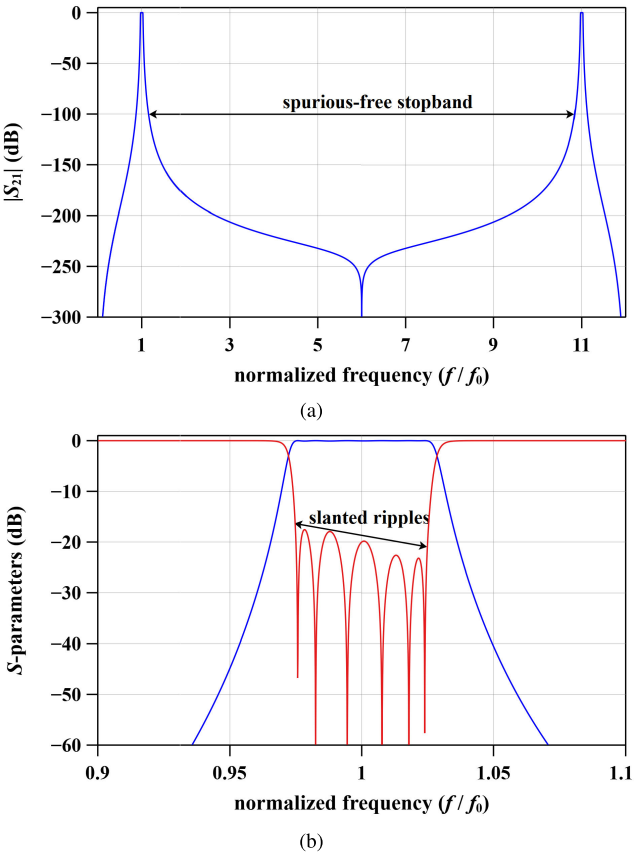

FIGURE 3. Response of the designed sixth-order filter. (a) Wide-range view of $|S_{21}|$. (b) Narrow-range view. Red line: $|S_{11}|$. Blue line: $|S_{21}|$.

acceptable exception is that the electrical lengths of the line components for implementing K_{23}, K_{45}, and so on, can be set to θ_c in place of $2\theta_c$. It can also be seen that there exists a transmission zero at $6f_0$. It naturally takes place due to the

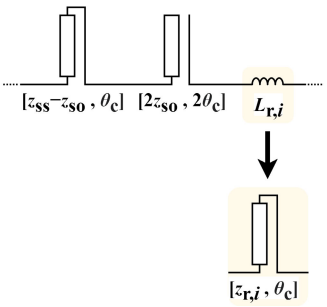

FIGURE 4. *i*th harmonic-controlled resonator loaded with a series inductor. Transformation scheme for the series inductor.

periodicity of the short-circuited series stubs in this filter. For example, six stubs in this filter have the input impedance of $j(70.85-5.086)\cdot\tan(f/f_0\cdot 15°)$ which becomes infinity at $6f_0$. This means that they become pure open circuits at $6f_0$, creating a transmission zero.

It can be seen in Fig. 3(b) that the filter does not produce an equi-ripple passband due to the frequency-variant features of the inverters in use. For example, the inverter structure utilized to implement the inverter of K_{12} yields the inverter value larger (smaller) than $|K_{12}|$ at frequencies right above (below) f_0, making the equi-ripple passband be slanted as shown in Fig. 3(b). The equi-ripple passband can be restored by trimming the resonant frequency of each resonator [15], *e.g.*, by intentionally loading a series inductor to each resonator as shown in Fig. 4. It is known that there does not exist a closed-form equation to compute the amount of the inductance to be loaded. By the aid of search algorithms, on the other hand, the optimum values of $L_{r,i}$, minimizing the cost function, can be identified. Our cost function is defined as the mean-squared error between the input impedance of the prespecified (ideal) Chebyshev filter and the input impedance of the circuit with frequency-variant (actual) inverters, sampled over the passband frequencies, *e.g.*, from $0.975f_0$ up to $1.025f_0$ for a filter having the fractional bandwidth of 0.05. This compensation technique has been demonstrated to be effective in restoring the equiripples of filters with a fractional bandwidth up to 0.5.

It is recommended to transform each loaded inductor into a θ_c-long series stub so that they can be absorbed into the adjoining resonators. The stub impedance is then

$$z_{r,i} = 2\pi f_0 L_{r,i}\cdot\cot\theta_c. \tag{7}$$

For demonstration, the inductor values and the characteristic impedances in Table 2 were obtained based on the approaches given above. Fig. 5 shows the response of the filter when its resonators are modified to have the structure shown in Fig. 4. Observe that the equi-ripple passband is restored as expected. The wide-range response is not shown since it is highly similar to the one in Fig. 3(a).

In order to obtain a physically-feasible schematic, it is required to further transform the stubs in Figs. 2 and 4 into coupled-transmission lines. For describing the transformation

TABLE 2. Parameter values of the modified sixth-order filter. Units for the inductor values are H. Units for the impedance-parameter values are Ω.

$L_{r,1}$ (=$L_{r,6}$)	$L_{r,2}$ (=$L_{r,5}$)	$L_{r,3}$ (=$L_{r,4}$)	$z_{r,1}$ (=$z_{r,6}$)	$z_{r,2}$ (=$z_{r,5}$)	$z_{r,3}$ (=$z_{r,4}$)
0.0059	0.0003	0	3.13	0.30385	2.16

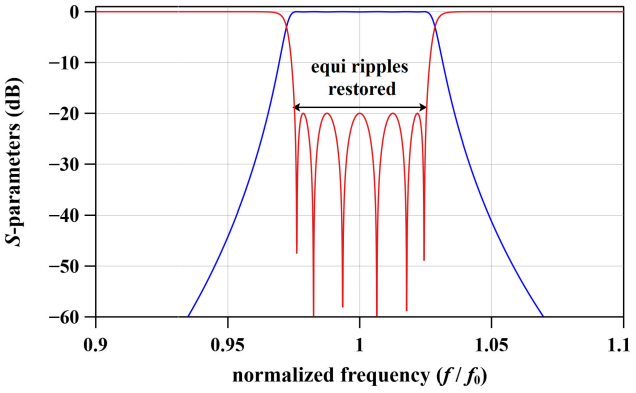

FIGURE 5. Response of the modified sixth-order filter. Red line: $|S_{11}|$. Blue line: $|S_{21}|$.

method, the circuit with the loaded stubs is drawn in Fig. 6. Equal-length stubs, *e.g.*, the short-circuited series stubs originating from the first resonator ($z_{ss}-z_{so}$), the inverter of K_{12} ($-z_{12}$), and the inductor for trimming the resonant frequency ($z_{r,1}$), are combined.

For transformation, θ_c-long line sections matched to the port impedance (z_0) have been inserted between each port and the first (last) resonator. A line section and an open-circuited series stub of equal length can be paired up and transformed into a coupled-line section followed by an impedance transformer as depicted in Fig. 6.

$$\begin{aligned} z_{e,1} &= z_0\cdot\left(1+\sqrt{\frac{z_0}{z_{u,1}+z_0}}\right)\\ z_{o,1} &= z_0\cdot\left(1-\sqrt{\frac{z_0}{z_{u,1}+z_0}}\right), \end{aligned} \tag{8a}$$

where

$$p = \sqrt{\frac{z_{u,1}}{z_0}+1}. \tag{8b}$$

Equation (8) again applies to the $(n+1)$th sub-circuit consisting of the nth open-circuited series stub. The two transformers can be removed from the schematic by scaling the impedances of the lines constituting the intermediate sections (sections 2 to n) by p^{-2}.

Each intermediate even-numbered sub-circuit (sub-circuits $2, 4, \ldots, n$) consists of three short-circuited stubs. In practice, the two series stubs are different in impedance as $z_{r,i}\neq z_{r,i+1}$ for most of the instances. Therefore, it is plausible to transform these sections into asymmetric-coupled line sections as shown in Fig. 6. For example, the four modal impedances of the asymmetric coupled-line section in sub-circuit 2 can be found as [16]

$$z_{ae,2} = z_{v,1} + 2z_{12}$$

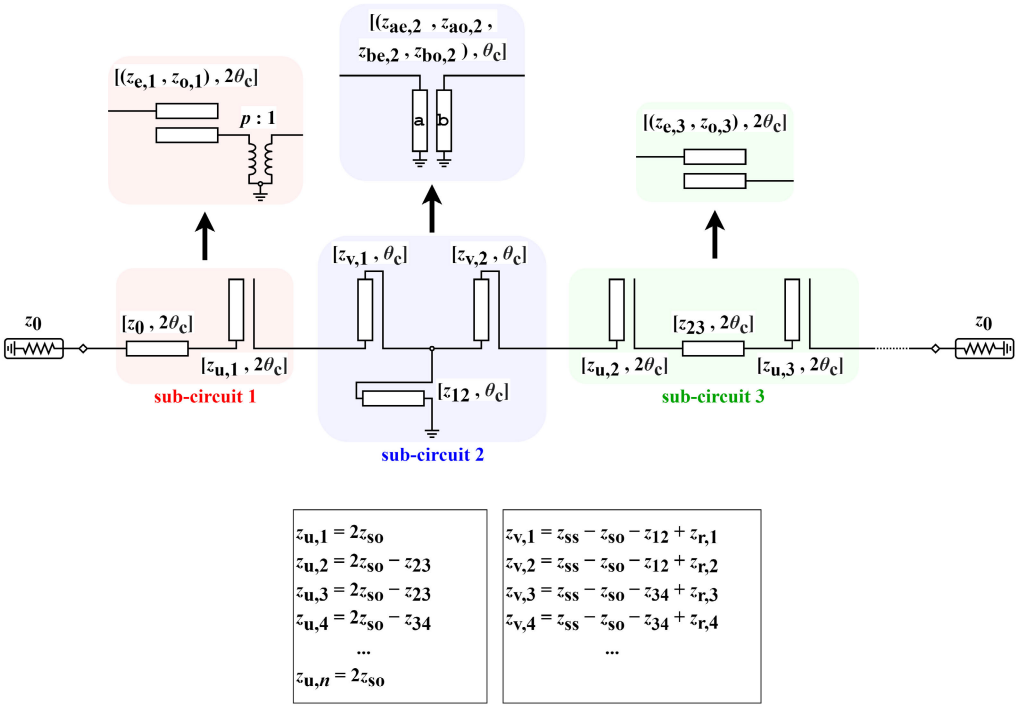

FIGURE 6. Circuit with loaded stubs and its transformation scheme.

$$\begin{aligned} z_{\mathrm{ao},2} &= z_{\mathrm{v},1} \\ z_{\mathrm{be},2} &= z_{\mathrm{v},2} + 2z_{12} \\ z_{\mathrm{be},2} &= z_{\mathrm{v},2}. \end{aligned} \tag{9}$$

Lastly, the remaining odd-numbered sub-circuits (sub-circuits 3, 5, …, $n-1$) can be transformed using the fact that two equal open-circuited series stubs and a line section in between are equivalent to a coupled-line section. Since the two open-circuited series stubs, *e.g.*, those in sub-circuit 3, are equal in impedance, symmetric coupled lines with the modal impedances of [17]

$$\begin{aligned} z_{\mathrm{e},3} &= z_{\mathrm{u},2} + 2z_{23}\ (= z_{\mathrm{u},3} + 2z_{23}) \\ z_{\mathrm{o},3} &= z_{\mathrm{u},2}\ (= z_{\mathrm{u},3}). \end{aligned} \tag{10}$$

appears.

The final coupled-line schematic and design parameters of the nth-order bandpass filter are shown in Fig. 7. It can be seen that the modal impedances of the coupled-line sections from 2 to n are scaled by p^{-2} to remove the transformers, as mentioned. It can be seen that the overall electrical size of the schematic depends on θ_{c}. Hence, having a smaller value of θ_{c} by setting m to a larger value [see (3)] leads to a filter schematic having a smaller size and producing a broader upper stopband.

For demonstration, three filters were designed to produce

- a fourth-order ($n = 4$) Chebyshev response with 20 dB-equi-ripple return loss;
- the fractional bandwidth of 0.05;
- the second passbands each centered at 6, 8, and $10f_0$ ($m = 6$, 8, and 10), respectively.

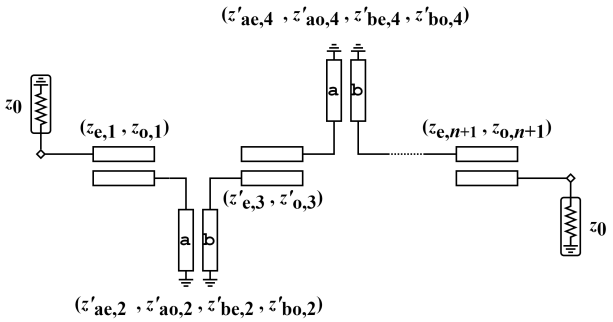

FIGURE 7. Coupled-line schematic.

The parameter values were computed under the condition that $z_0 = 50\ \Omega$. The computed parameter values are summarized in Table 3. The responses of the designed filters are plotted in Fig. 8. It can be observed that all three coupled-line filters produce the prespecified response, validating our design approach.

C. DUAL SCHEMATIC

The design approach discussed in Section II used prototype circuits made of series-LC resonators and impedance

TABLE 3. Parameter values of the designed fourth-order filters. Units for the impedance-parameter values are Ω.

m	θ_c	$z_{e,1}$ (=$z_{e,5}$)	$z_{o,1}$ (=$z_{o,5}$)	$z'_{ae,2}$ (=$z'_{be,4}$)	$z'_{ao,2}$ (=$z'_{bo,4}$)	$z'_{be,2}$ (=$z'_{ae,4}$)	$z'_{bo,2}$ (=$z'_{ae,4}$)	$z'_{e,3}$	$z'_{o,3}$
6	25.714°	62.251	37.749	83.352	72.759	83.125	72.532	48.530	45.467
8	20°	63.603	36.397	160.623	143.340	160.238	142.956	47.852	44.746
10	16.364°	64.825	35.175	254.987	229.543	254.395	228.951	47.157	44.052

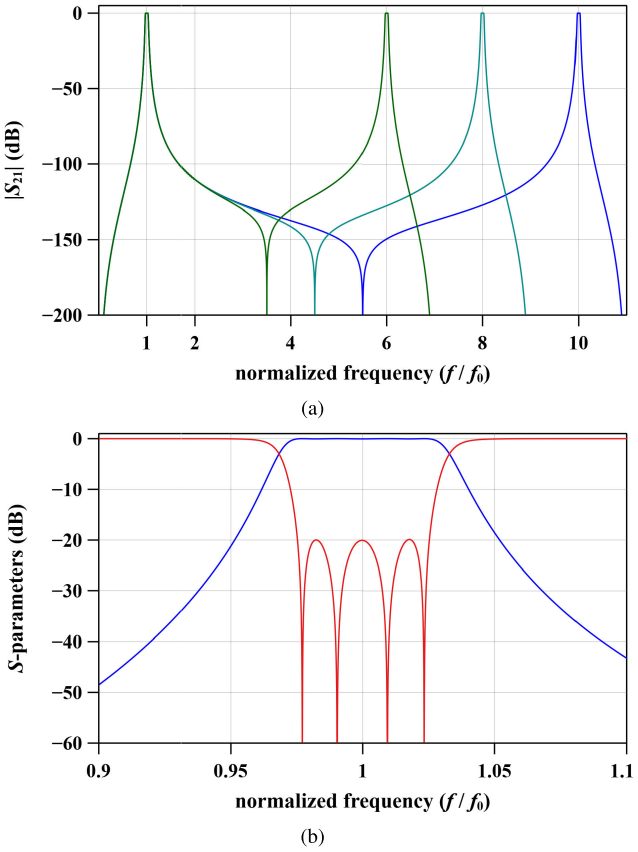

FIGURE 8. Responses of the designed fourth-order filters. (a) Wide-range view of $|S_{21}|$. Green, cyan, and blue lines: $|S_{21}|$ of the filters with $m = 6$, 8, and 10, respectively. In order to provide a clear view, the responses are each plotted up to the frequency at which the second passband ends. (b) Near-center response of the filter with $m = 10$. Red lines: $|S_{11}|$. Blue lines: $|S_{21}|$. Those of the filters with $m = 6$ and 8 are highly indistinguishable from it.

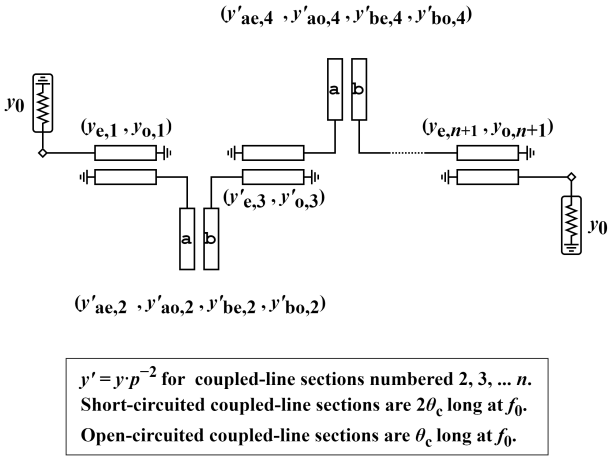

FIGURE 9. Coupled-line schematic dual to the one shown in Fig. 7.

inverters. This led to the coupled-line schematic shown in Fig. 7, and it can be seen from Table 3 that filters designed based on this schematic have coupled-line sections with large modal impedances, especially when m is set to a large value.

Alternatively, the use of high-impedance coupled-line sections can be avoided by using another schematic that originates from a prototype made of parallel-LC resonators and admittance inverters, which is the dual of the one shown in Fig. 2. This dual schematic is shown in Fig. 9. Owing to the duality conditions, the design equations can be obtained by using (4b) instead of (4a) and by changing the impedance parameters in (5)-(10) (*e.g.* K, z, L, and, z') into admittance parameters (J, y, C, and, y'). The type of connection (series to shunt) and termination (open circuit to short circuit) of the stubs should also be exchanged in whole.

For demonstration, three filters were designed to produce

- a fourth-order (n = 4) Chebyshev bandpass response with 0.1 dB-equi-ripple passband;
- the fractional bandwidth of 0.1;
- the second passbands each centered at 5, 7, and 9f_0 (m = 5, 7, and 9), respectively.

The parameter values were computed under the condition that $y_0 = 0.02\ \Omega^{-1}$. The computed parameter values are summarized in Table 4. It can be seen that the modal admittances tend to increase with m, *i.e.*, the modal impedances decrease as m increases.

The responses of the designed filters are shown in Fig. 10, and they validate the schematic shown in Fig. 9. In brief, one may choose either of the schematics in filter designs considering physical structures of transmission lines (*e.g.,* microstrip lines, slot lines, or coplanar waveguides), environment of the medium, and so on.

III. FILTER EXAMPLES

The first subsection is to verify the coupled-line schematic in Fig. 7 using single-layer microstrip lines. Practical multilayer filters will be presented in the following subsection with the discussions on the effects of choosing a large m in (1) on actual filter responses.

A. SINGLE-LAYER MICROSTRIP-LINE FILTER EXAMPLE

For verification, a single-layer microstrip-line filter was implemented, fabricated, and measured. It was implemented

TABLE 4. Parameter values of the designed fourth-order filters. Units for the admittance-parameter values are Ω^{-1}.

m	θ_c	$y_{e,1}$ (=$y_{e,5}$)	$y_{o,1}$ (=$y_{o,5}$)	$y'_{ae,2}$ (=$y'_{be,4}$)	$y'_{ao,2}$ (=$y'_{bo,4}$)	$y'_{be,2}$ (=$y'_{ae,4}$)	$y'_{bo,2}$ (=$y'_{ae,4}$)	$y'_{e,3}$	$y'_{o,3}$
5	30°	0.014625	0.025375	0.016406	0.021016	0.016250	0.020861	0.017643	0.019468
7	22.5°	0.013979	0.026021	0.040153	0.048218	0.039875	0.047940	0.017252	0.019122
9	18°	0.013398	0.026602	0.069740	0.082099	0.069310	0.081669	0.016887	0.018755

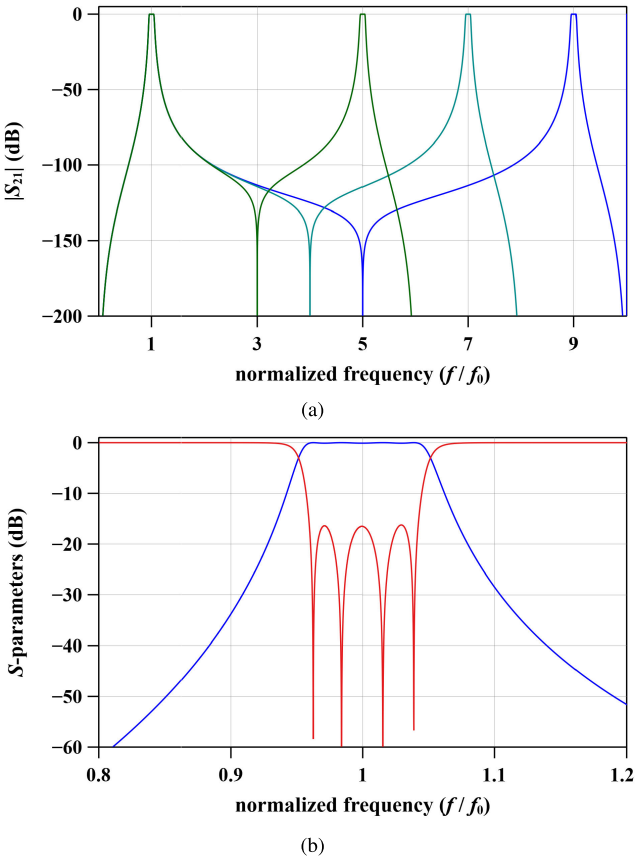

FIGURE 10. Responses of the designed fourth-order filters. (a) Wide-range view of $|S_{21}|$. Green, cyan, and blue lines: $|S_{21}|$ of the filters with $m = 5$, 7, and 9, respectively. In order to provide a clear view, the responses are each plotted up to the frequency at which the second passband ends. (b) Near-center response of the filter with $m = 9$. Red lines: $|S_{11}|$. Blue lines: $|S_{21}|$. Those of the filters with $m = 5$ and 7 are highly indistinguishable from it.

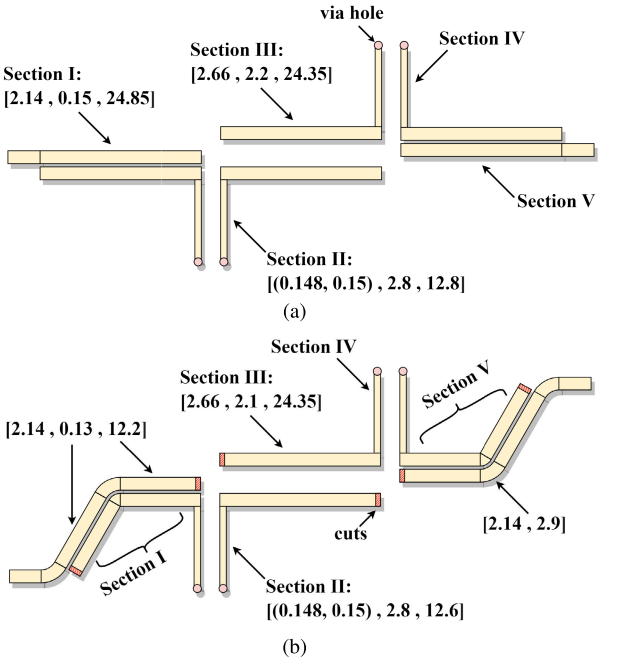

FIGURE 11. Physical schematics of the single-layer microstrip-line filter (not to scale). [n_1, n_2, n_3]: [width, spacing, length]. [(n_1, n_2), n_3, n_4]: [(width of line 'a', width of line 'b'), spacing, length]. [n_1, n_2]: [width, length]. Units: mm. Each schematic has odd symmetry. (a) Initial schematic. (b) Modified schematic. Cuts are no longer than 0.2 mm.

based on the schematic in Fig. 7 and the parameter values in the second row of Table 3. f_0 was set to 1 GHz. A 31-mil thick Rogers 5880 substrate ($\varepsilon_r = 2.2$, $\tan\delta = 0.0009$) was utilized.

Fig. 11(a) shows the initial physical schematic. Its dimensions were obtained by plugging the aforementioned parameter values and the properties of the substrate into a line calculator tool. In other words, there was no need to execute trial-and-error coupling tests to find the initial dimensions of the filter.

The initial schematic in Fig. 11(a) was modified to the one in Fig. 11(b), considering the parasitics and non-idealities of physical microstrip lines. The lengths and spacings of the coupled-line sections were reduced to compensate the parasitic effects (*e.g.*, open-end effects and via-hole inductance) and discontinuities such as impedance steps.

Microstrip coupled lines have unequal even- and odd-mode phase constants [18]. Due to this deviation, a typical microstrip coupled-line filter produces unintended spurious peaks in its stopband, and the coupled-line sections with tight spacings are the main contributors. In the initial schematic in Fig. 11(a), sections I and V were identified as the significant contributors. In order to remove these peaks, these sections were modified to as shown in Fig. 11(b). Details on the method for adjusting their dimensions will not be discussed in this article as they are available in [19].

Comparison between the initial and final dimensions discloses that only minor adjustments have been made. In fact, it is a common practice to make such adjustments when designing microstrip-line filters, since line calculator tools typically provide dimensions based on idealized conditions and do not take into account the parasitics and non-idealities that can affect the electrical properties of the lines.

Fig. 12 shows the photograph of the filter fabricated based on the physical schematic in Fig. 11(b). As mentioned

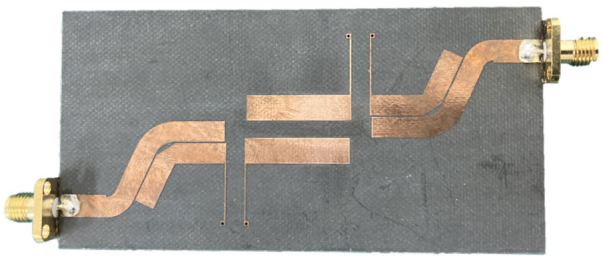

FIGURE 12. Photograph of the fabricated single-layer microstrip-line filter.

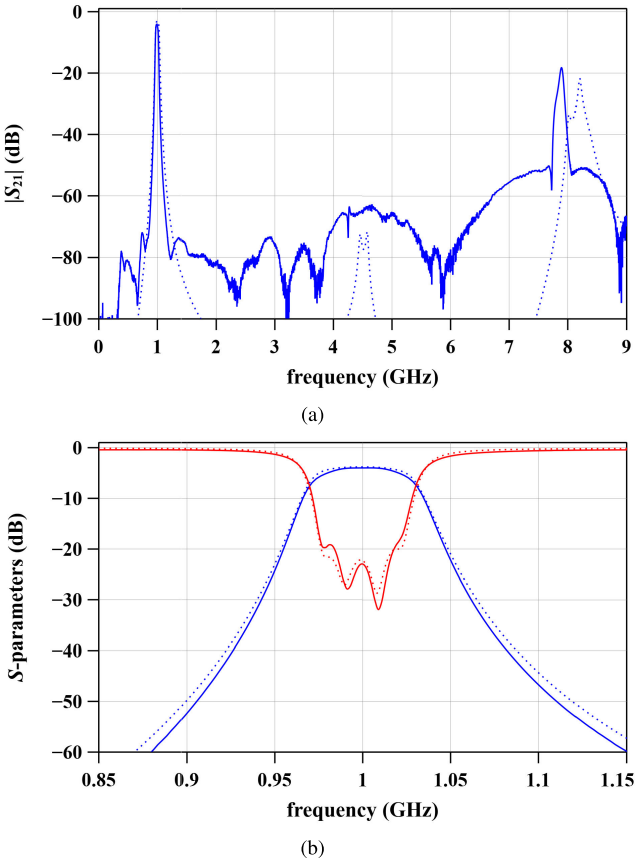

FIGURE 13. Responses of the single-layer microstrip-line filter. Solid lines: measured response. Dotted lines: EM-simulated response. (a) Wide-range view of $|S_{21}|$. (b) Narrow-range view. Red lines: $|S_{11}|$. Blue lines: $|S_{21}|$.

previously, having a large m (m = 8) to acquire a broad upper-stopband resulted in the emergence of high-impedance lines (narrow-strip-width lines). This becomes the limiting factor of circuit fabrication when the lines are on a uniform, single-layer dielectric substrate. Our solutions to such issue will be discussed in Section III-B.

The measured S-parameters of the fabricated microstrip-line filter is shown in Fig. 13 along with its EM simulation results. Its target response can be found in Fig. 8. It can be seen that the first-harmonic passband occurs near 8 GHz (=$8f_0$), creating a spotless upper-stopband ($|S_{21}| < -60$ dB) up to $8f_0$.

One of the downsides of having a large m can be identified by observing the passband response of the filter shown in Fig. 12(b). It reveals that the fabricated filter has the insertion loss of 4.1 dB, agreeing with the EM simulation (4.0 dB when σ is set to $5.8{\cdot}10^7$ S/m). One might expect an insertion loss near 2 dB (postulating $Q_u = 200$) for a microstrip half-wavelength-resonator filter having the same fractional bandwidth as the fabricated filter. This increase in the insertion loss can be attributed to two facts that

1) the average length of the coupled-line sections (30° at f_0) is three times shorter than that of conventional, half-wavelength coupled-line filters (90° at f_0);
2) the increase in the conductor loss as a result of the use of narrow lines (high-impedance lines).

Therefore, the compromise between the insertion loss and the location of the second passband must be carried out in filter designs. In addition, it is suggested to use a line structure capable of implementing a high characteristic impedance without having a narrow width (*e.g.*, a microstrip line on a thick, low-dielectric-constant substrate).

B. LTCC-PROCESSED MULTI-LAYER FILTER EXAMPLES

Stacking up multiple dielectric layers in organizing coupled-line filters allows us to have

- capability to form large couplings that cannot be obtained by placing the lines side by side (*e.g.* edge couplings);
- easy and dynamic control on the characteristic impedance of a transmission line that enables to overcome fabrication limits (*e.g.* lines having extremely narrow strip widths),

both of which facilitate filter realization with a large bandwidth and a broad upper stopband.

For the purpose of demonstrating the insertion-loss variation with the location of the first harmonic (mf_0), two multi-layer filters were designed using the parameters values in the first and the second rows of Table 4. f_0 of these filters was set to 2 GHz.

The overall structure of the LTCC filters is shown in Fig. 14(a). Three dielectric layers, each having ε_r of 6.2 and $\tan\delta$ of 0.0013, were stacked up to formulate a four-conductor (including the ground) microstrip environment. Conductor layers 1 and 2 were intended to be separated by the minimum available substrate thickness of 0.1 mm to maximize the available amount of couplings between a pair of broadside-coupled lines. The bottom-most dielectric layer was also determined to be 0.1-mm thick to make conductor layer 3 be closest, to the fullest extent, to the ground. Hence, it is evident that high-admittance coupled-line sections would have feasible dimensions when placed at conductor layer 3.

The physical schematics and the photograph of the fabricated filters are shown in Fig. 14(b). Their dimensions are summarized in Table 5. It informs that the widths of the lines are proximate to one another.

Fig. 15 shows the measured responses of the filters. Their second passbands, which are trampled due to the

TABLE 5. Dimensions of the fabricated LTCC filters. Units: mm.

m	$w_{1,1}$	$w_{1,2}$	$w_{2,a}$	$w_{2,b}$	w_3	w_c	s_1	s_2	s_3	$l_{1,1}$	$l_{1,2}$	l_2	l_3	l_c
5	0.47	0.28	0.28	0.27	0.29	0.47	0.46	0.31	0.76	5.58	5.03	6.45	9.88	0.91
7	0.43	0.24	0.35	0.34	0.27	0.43	0.39	0.15	0.74	4.30	3.86	3.75	7.65	0.72

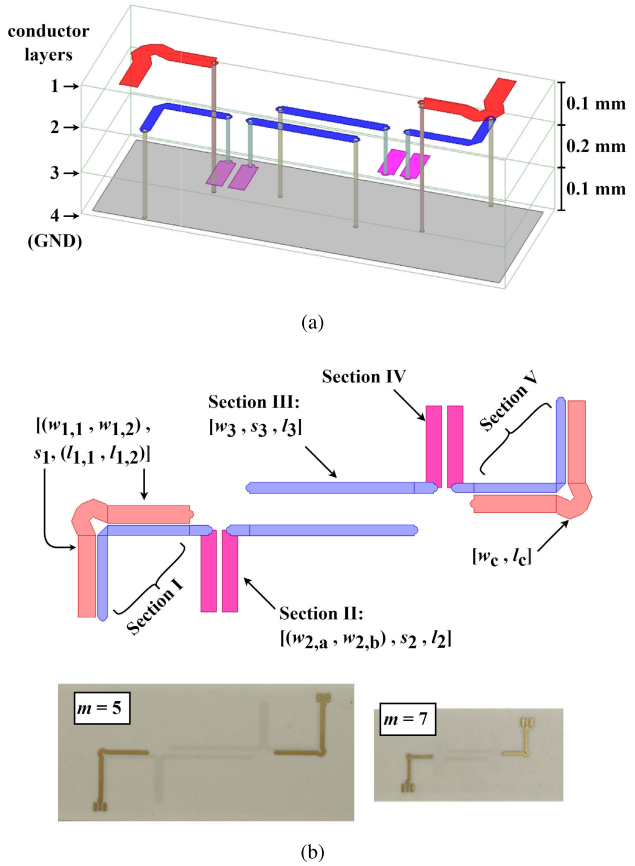

FIGURE 14. Multi-layer LTCC filters. Not to scale. (a) Bird-eye view. (b) Top-views of the physical schematic and the fabricated filters. The schematic is radially symmetric to its center.

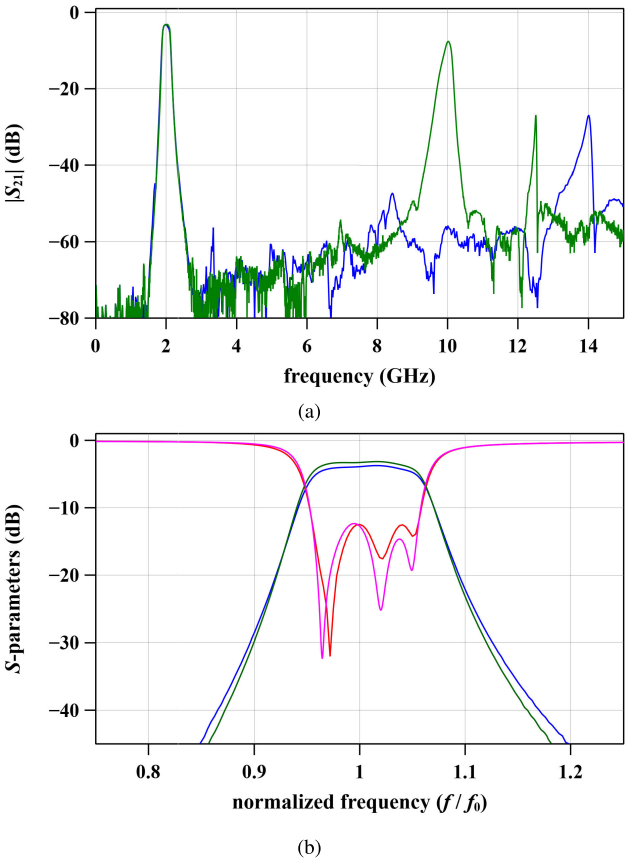

FIGURE 15. Measured responses of the fabricated LTCC filters. Green and blue lines: $|S_{21}|$ of the filters with $m = 5$ and 7, respectively. (a) Wide-range view of $|S_{21}|$. (b) Responses in the normalized frequency domain to observe the insertion loss variation with m. Magenta and red lines: $|S_{11}|$ of the filters with $m = 5$ and 7, respectively.

insertion loss and imperfect dimensions, appear at 10 ($=5f_0$) and 14 GHz ($=7f_0$) as expected. The plot for the filter with $m = 5$ shows an additional peak around 12.5 GHz, which can be attributed to a higher-order harmonic of the filter. Nonetheless, the plots clearly indicate that our approach and schematic facilitate designing a filter with the second passband centered at a designated frequency.

Fig. 15(b) compares the passbands of the filters with $m = 5$ and 7. Their insertion losses were measured to be 2.4 dB ($m = 5$) and 2.8 dB ($m = 7$), each of which coincides with the insertion loss of a filter comprising resonators of $Q_u = 100$ and 80, respectively. A typical microstrip coupled-line line filter having the same specification as the fabricated filters was theoretically estimated to have an insertion loss of 1.8 dB ($Q_u = 130$) when it is implemented on conductor layer 1.

IV. CONCLUSION

This article discussed a synthesis (finding the schematic and its electrical parameters) method for a transmission-line filter whose second passband can be placed at any multiple of the center frequency, in theory. Detailed discussions on harmonic-controlled resonator structures were given as well as their applications to actual filter designs. Practical coupled-line schematics for harmonic-controlled filters were derived based on rigorous circuit transformations. Our closed-form equations for the design parameters led us design harmonic-controlled filters with different specifications in a straightforward manner. In other words, the dimensions of our filters were found without carrying out coupling tests, which highlighted our design approach.

A single-layer and two multi-layer filters were designed and fabricated for validation, and the measurement results

TABLE 6. Parameter values of the designed fourth-order filters. Units for the impedance-parameter values are Ω.

m	θ_c	$z_{e,1}$ (=$z_{e,5}$)	$z_{o,1}$ (=$z_{o,5}$)	$z'_{ae,2}$ (=$z'_{be,4}$)	$z'_{ao,2}$ (=$z'_{bo,4}$)	$z'_{be,2}$ (=$z'_{ae,4}$)	$z'_{bo,2}$ (=$z'_{ae,4}$)	$z'_{e,3}$	$z'_{o,3}$
6	25.714°	66.827	33.173	201.632	181.646	201.171	181.185	45.942	42.732
8	20°	68.563	31.437	342.247	310.065	341.498	309.316	44.648	41.568
10	16.364°	70.101	29.899	510.682	463.906	509.592	462.817	43.406	40.432

showed excellent agreements with the theory. It has been verified that the high-immittance lines did not hinder the circuit realization when a multi-layer structures was used for implementing the coupled-line schematics with a large m. Our analysis on actual filter responses pointed out that the compromise between the insertion loss and the location of the second passband (mf_0) must be made in the design of harmonic-controlled filters.

Although this work focuses on basic harmonic-controlled filter designs based on direct-coupled filter topologies, our theoretical framework can also be applied to the design of more advanced filters. This may involve using complex filter topologies, a variety of inverter structures as well as resonator structures, and other coupled-line transformations beyond those presented in this article. Nonetheless, it is important to note that the proposed schematic-formulation concept offers a valuable starting point for further exploration of the potential of the harmonic-controlled resonator structures in designing harmonic-controlled filters with diverse and interesting features.

APPENDIX I

This section is to discuss how to formulate filter schematics using the harmonic-controlled resonators shown in the third column of Fig. 1. It is worth noting that the method, process, and resulting schematics are almost identical to those discussed in Section II-B.

Fig. 16(a) shows the circuit formulated by using the resonator structure shown in the first row-third column of Fig. 1. This circuit can be derived from the prototype circuit in Fig. 2 using the approach described earlier in Section II-B with one exception: the electrical lengths of the lines used to implement the inverters of K_{23}, K_{45}, and so on, are set to θ_c instead of $2\theta_c$. Therefore, the design formulas in (5)-(7) can be reused, while replacing $2\theta_c$ in (6) with θ_c.

Fig. 16(b) shows the schematic derived from the circuit in Fig. 16(a). The approach used to formulate this schematic is the same as discussed earlier in Section II-B. This indicates that the impedance parameters in Fig. 16(b) can be obtained from the ones in Fig. 16(a) by simply reusing (8)-(10).

By comparing the schematics in Figs. 7 and 16(b), one can identify that the one in Fig. 16(b) has a smaller electrical size than the one in Fig. 7. However, this advantage in size comes with a critical drawback related to fabrication difficulty.

In order to discuss it in depth, three filters were designed based on the schematic in Fig. 16(b) to produce the fourth-order responses that are identical to the ones described in Section II-B. Their parameter values were calculated for $z_0 = 50\ \Omega$, and are summarized in Table 6. Their responses are not shown since they are almost indistinguishable from those plotted in Fig. 8. By comparing the values in Tables 3 and 6, one can confirm that the filters designed based on the schematic in Fig. 16(b) have lines with higher modal impedances than those designed based on the schematic in Fig. 7. This concludes that using the schematic in Fig. 16(b) may not be encouraged, as it necessitates implementing physical lines of which the impedances are unnecessarily high.

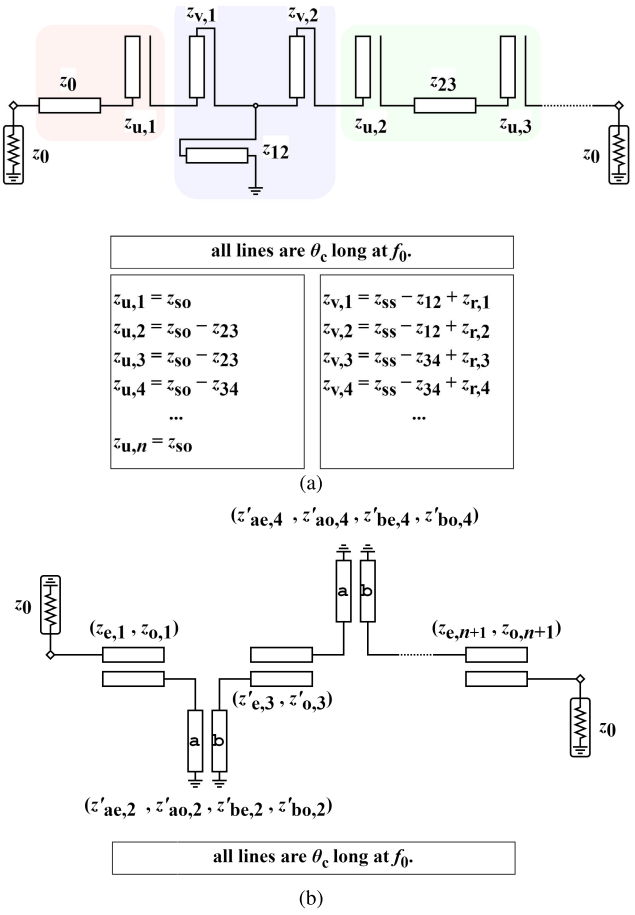

FIGURE 16. Stub circuit and schematic obtained by using harmonic-controlled resonator structure in the first row-third column in Fig. 1. (a) Stub circuit corresponding to the one in Fig. 6. (b) Schematic corresponding to the one in Fig. 7.

APPENDIX II

A. DESIGN PROCEDURE

This section provides the detailed procedure for designing harmonic-controlled filters. The procedure can be broken down into the following steps:

1) Synthesize the bandpass prototype circuit shown in Fig. 2.
2) Determine m and synthesize the stub circuit that corresponds to the prototype circuit.
3) (optional) Load an inductor onto each resonator, find the optimum inductor values, and transform the loaded inductors into short-circuited stubs.
4) Find the modal impedances of the coupled-line sections in the schematic shown in Fig. 7.

The order, response type, and fractional bandwidth of a filter are determined in the first step. For example, the design formulas for the sixth-order prototype circuit are given as

$$\begin{aligned} L_s &= \frac{1}{2\pi f_0} \cdot \frac{z_0 \cdot g_1}{\Delta} \\ C_s &= \frac{1}{2\pi f_0} \cdot \frac{\Delta}{z_0 \cdot g_1} \\ K_{12} &= z_0 \cdot \sqrt{\frac{g_1}{g_2}} \\ K_{23} &= z_0 \cdot \frac{g_1}{\sqrt{g_2 \cdot g_3}} \\ K_{34} &= z_0 \cdot \frac{g_1}{\sqrt{g_3 \cdot g_4}} \\ K_{45} &= z_0 \cdot \frac{g_1}{\sqrt{g_4 \cdot g_5}} \\ K_{56} &= z_0 \cdot \frac{g_1}{\sqrt{g_5 \cdot g_6}}, \end{aligned} \tag{11}$$

where $g_1, g_2, \ldots, g_6$ denote the normalized filter parameters (a.k.a. g-parameters) that determine the response type and Δ denotes the fractional bandwidth. For example, when the normalized filter parameters are set to the values for a Chebyshev filter with 20-dB equi-ripple return loss (g_1 = 0.9958, g_2 = 1.4131, g_3 = 1.8950, g_4 = 1.5505, g_5 = 1.7272, and g_6 = 0.8147), Δ is set to 0.05, and z_0 is set to 1 Ω, the design parameters then become

$$\begin{aligned} L_s &= \frac{3.1697}{f_0}\ \text{H} \\ C_s &= \frac{7.9913}{f_0}\ \text{mF} \\ K_{12} &= K_{56} = 0.8394\ \Omega \\ K_{23} &= K_{45} = 0.6085\ \Omega \\ K_{34} &= 0.5809\ \Omega. \end{aligned} \tag{12}$$

A prototype circuit having a different response type (*e.g.*, Butterworth response or Chebyshev responses with different levels of equi ripples) and different fractional bandwidth can be synthesized by setting the normalized filter parameters and Δ accordingly.

The center frequency of the second passband (mf_0) is determined in the second step. The design parameters of the stubs originating from the series-*LC* resonators can be determined using (2a), (3), and (4a), and the characteristic impedances of the lines originating from the inverters can be determined using (5) and (6). For example, when m is set to 11, the design parameters of the lines originating from the series-*LC* resonators and inverters of (12) are calculated to be the ones listed in Table 1.

The third step can be omitted if the slant in the return-loss ripples is tolerable. In fact, if there are no inductors loaded onto the resonators, it is possible to avoid using asymmetric coupled lines. Since this work has shown various designs that incorporated these inductors, we will proceed this design without the use of loaded inductors.

Finally, in the fourth step, the design parameters of the schematic can be determined by 1) using (8)-(10) and 2) scaling the modal impedances of the intermediate coupled-line sections by p^{-2}. For example, plugging the parameter values

TABLE 7. Schematic and parameter values for a second-order filter (response type: Chebyshev response with 20-dB equi-ripple return loss). Units for the impedance-parameter values are Ω.

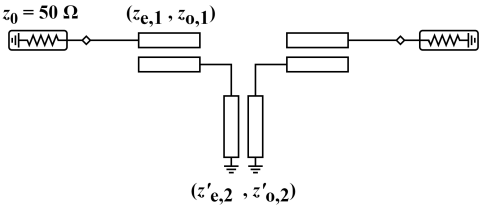

Schematic has even symmetry.
Open-circuited coupled-line sections are $2\theta_c$ long at f_0.
Short-circuited coupled-line sections are θ_c long at f_0.

Δ	m	θ_c	$z_{e,1}$	$z_{o,1}$	$z'_{e,2}$	$z'_{o,2}$
0.05	5	30°	63.493	36.507	53.456	39.522
	6	25.714°	64.323	35.677	85.591	66.768
	7	22.5°	65.114	34.886	122.091	97.727
	8	20°	65.862	34.138	162.811	132.242
	9	18°	66.570	33.430	207.577	170.209
0.1	5	30°	68.422	31.578	56.958	30.937
	6	25.714°	69.473	30.527	88.656	53.793
	7	22.5°	70.460	29.540	124.138	79.387
	8	20°	71.382	28.618	163.145	107.544
	9	18°	72.244	27.756	205.490	138.082
0.15	5	30°	71.834	28.166	61.189	24.360
	6	25.714°	72.993	27.007	92.820	43.862
	7	22.5°	74.071	25.929	127.804	65.427
	8	20°	75.066	24.934	165.839	88.862
	9	18°	75.987	24.013	206.661	114.011
0.2	5	30°	74.447	25.553	62.540	16.923
	6	25.714°	75.662	24.338	93.406	33.076
	7	22.5°	76.779	23.221	127.131	50.749
	8	20°	77.803	22.197	163.522	69.719
	9	18°	78.741	21.259	202.200	89.889

TABLE 8. Schematic and parameter values for a fourth-order filter (response type: Chebyshev response with 20-dB equi-ripple return loss). Units for the impedance-parameter values are Ω.

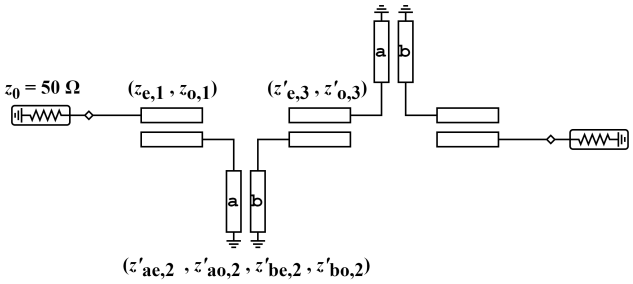

Schematic has odd symmetry.
Open-circuited coupled-line sections are $2\theta_c$ long at f_0.
Short-circuited coupled-line sections are θ_c long at f_0.

Δ	m	θ_c	$z_{e,1}$	$z_{o,1}$	$z'_{ae,2}$	$z'_{ao,2}$	$z'_{be,2}$	$z'_{bo,2}$	$z'_{e,3}$	$z'_{o,3}$
0.05	5	30°	61.524	38.476	51.417	43.597	51.253	43.434	48.845	45.842
	6	25.714°	62.251	37.749	83.352	72.759	83.125	72.532	48.530	45.467
	7	22.5°	62.944	37.056	119.799	106.049	119.495	105.746	48.196	45.102
	8	20°	63.603	36.397	160.623	143.340	160.238	142.956	47.852	44.746
	9	18°	64.230	35.770	205.726	184.543	205.240	184.057	47.504	44.396
0.1	5	30°	65.882	34.118	53.010	38.160	52.380	37.531	47.802	42.108
	6	25.714°	66.827	33.173	84.285	64.299	83.414	63.428	47.222	41.451
	7	22.5°	67.721	32.279	119.575	93.803	118.433	92.661	46.613	40.824
	8	20°	68.563	31.437	158.692	126.510	157.240	125.058	45.994	40.221
	9	18°	69.355	30.645	201.443	162.251	199.660	160.469	45.377	39.637
0.15	5	30°	68.978	31.022	54.738	33.533	53.399	32.194	46.846	38.743
	6	25.714°	70.049	29.951	85.535	57.163	83.672	55.300	46.041	37.876
	7	22.5°	71.053	28.947	119.933	83.560	117.496	81.123	45.205	37.061
	8	20°	71.990	28.010	157.696	112.536	154.629	109.468	44.365	36.288
	9	18°	72.864	27.136	198.606	143.917	194.858	140.169	43.535	35.550
0.2	5	30°	71.406	28.594	56.609	29.631	54.324	27.347	45.962	35.696
	6	25.714°	72.554	27.446	87.043	51.138	83.904	47.998	44.966	34.674
	7	22.5°	73.622	26.378	120.746	74.955	116.663	70.872	43.939	33.727
	8	20°	74.611	25.389	157.459	100.891	152.334	95.767	42.918	32.841
	9	18°	75.527	24.473	196.923	128.755	190.682	122.514	41.915	32.007

in Table 1 into (8)-(10) gives

$$
\begin{aligned}
p &= 3.3454 \\
z_{e,1} &= z_{e,7} = 1.2989\ \Omega \\
z_{o,1} &= z_{o,7} = 0.7011\ \Omega \\
z_{ae,2} &= z_{be,2} = z_{ae,6} = z_{be,6} = 69.1444\ \Omega \\
z_{ao,2} &= z_{bo,2} = z_{ao,6} = z_{bo,6} = 62.7487\ \Omega \\
z_{e,3} &= z_{e,5} = 10.4962\ \Omega \\
z_{o,3} &= z_{o,5} = 9.8876\ \Omega \\
z_{ae,4} &= z_{be,4} = 68.0496\ \Omega \\
z_{ao,4} &= z_{bo,4} = 63.7134\ \Omega
\end{aligned} \tag{13}
$$

Scaling the values of the parameters with subscripts 2, 3, 4, 5, and 6 by $p^{-2} = 0.08935$ gives

$$
\begin{aligned}
z'_{ae,2} &= z'_{be,2} = z'_{ae,6} = z'_{be,6} = 6.1665\ \Omega \\
z'_{ao,2} &= z'_{bo,2} = z'_{ao,6} = z'_{bo,6} = 5.6066\ \Omega \\
z'_{e,3} &= z'_{e,5} = 0.9378\ \Omega \\
z'_{o,3} &= z'_{o,5} = 0.8835\ \Omega \\
z'_{ae,4} &= z'_{be,4} = 6.0803\ \Omega \\
z'_{ao,4} &= z'_{bo,4} = 5.6928\ \Omega
\end{aligned} \tag{14}
$$

As previously stated when discussing the third step, coupled-line sections 2, 4, 6 are no longer asymmetric. The designed filter produce a response that is identical to the one shown in Fig. 3.

TABLE 9. Schematic and parameter values for a sixth-order filter (response type: Chebyshev response with 20-dB equi-ripple return loss). Units for the impedance-parameter values are Ω.

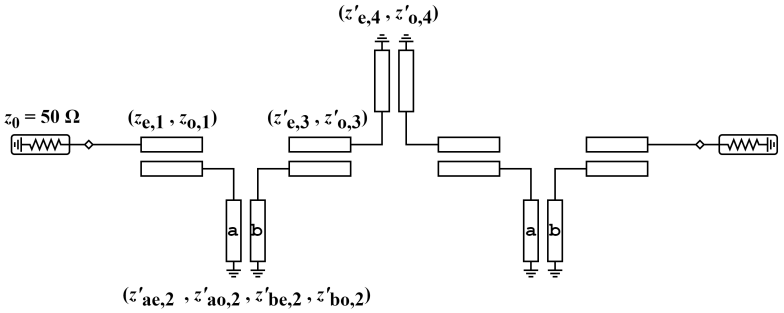

Schematic has even symmetry.
Open-circuited coupled-line sections are $2\theta_c$ long at f_0.
Short-circuited coupled-line sections are θ_c long at f_0.

Δ	m	θ_c	$z_{e,1}$	$z_{o,1}$	$z'_{ae,2}$	$z'_{ao,2}$	$z'_{be,2}$	$z'_{bo,2}$	$z'_{e,3}$	$z'_{o,3}$	$z'_{e,4}$	$z'_{o,4}$
0.05	5	30°	61.175	38.825	51.284	44.021	51.145	43.882	48.817	46.187	50.008	44.986
	6	25.714°	61.882	38.118	83.250	73.406	83.059	73.216	48.518	45.834	81.520	74.715
	7	22.5°	62.557	37.443	119.756	106.973	119.507	106.725	48.202	45.491	117.509	108.674
	8	20°	63.200	36.800	160.681	144.607	160.367	144.293	47.877	45.154	157.855	146.746
	9	18°	63.811	36.189	205.915	186.204	205.529	185.818	47.548	44.822	202.450	188.828
0.1	5	30°	65.424	34.576	52.720	38.885	52.196	38.361	47.745	42.739	49.990	40.433
	6	25.714°	66.348	33.652	84.041	65.406	83.313	64.678	47.193	42.116	80.349	67.482
	7	22.5°	67.224	32.776	119.431	95.382	118.474	94.425	46.615	41.518	114.660	98.060
	8	20°	68.049	31.951	158.693	128.639	157.488	127.434	46.029	40.940	152.737	131.984
	9	18°	68.826	31.174	201.671	165.044	200.185	163.558	45.442	40.380	194.405	169.104
0.15	5	30°	68.456	31.544	54.293	34.483	53.167	33.357	46.759	39.613	49.942	36.302
	6	25.714°	69.508	30.492	85.115	58.581	83.561	57.027	45.987	38.787	79.266	61.001
	7	22.5°	70.496	29.504	119.591	85.539	117.582	83.529	45.191	38.003	112.078	88.652
	8	20°	71.419	28.581	157.559	115.236	154.993	112.670	44.391	37.255	148.179	119.050
	9	18°	72.281	27.719	198.698	147.394	195.588	144.284	43.601	36.538	187.334	152.032
0.2	5	30°	70.843	29.157	55.950	30.684	54.058	28.792	45.853	36.762	49.864	32.502
	6	25.714°	71.975	28.025	86.413	52.743	83.791	50.121	44.896	35.779	78.233	55.132
	7	22.5°	73.030	26.970	120.218	77.223	116.792	73.797	43.917	34.859	109.737	80.210
	8	20°	74.009	25.991	157.044	103.867	152.796	99.618	42.938	33.996	144.086	107.586
	9	18°	74.917	25.083	196.709	132.550	191.573	127.414	41.982	33.175	181.078	137.059

Overall, this procedure provides a systematic way for designing harmonic-controlled filters, allowing for customizing the response type, the fractional bandwidth, and the location of the second passband.

B. DESIGN TABLES

This section provides design tables for the harmonic-controlled filters. The tables summarize parameter values for several harmonic-controlled filters, covering a broad range of filter orders, fractional bandwidths, and m. By virtue of these tables, one may quickly use the appropriate parameter values in filter designs, thus saving time and effort in the design process.

Filters in these tables can be implemented on a 100-mil thick substrate of $\varepsilon_r = 2.2$ without having lines that are narrower and/or spaced tighter than 0.05 mm. Considering that

1) having a larger value of m necessitates implementing narrower lines;
2) having a larger value of Δ leads to the need for implementing lines that are spaced tighter,

it is not recommended to implement filters having larger values of m and Δ than those shown in these tables using single-layer microstrip lines. However, this should not be mistaken as a limitation of our design approach, since they can still be implemented without having extreme

TABLE 10. Schematic and parameter values for an eighth-order filter (response type: Chebyshev response with 20-dB equi-ripple return loss). Units for the impedance-parameter values are Ω.

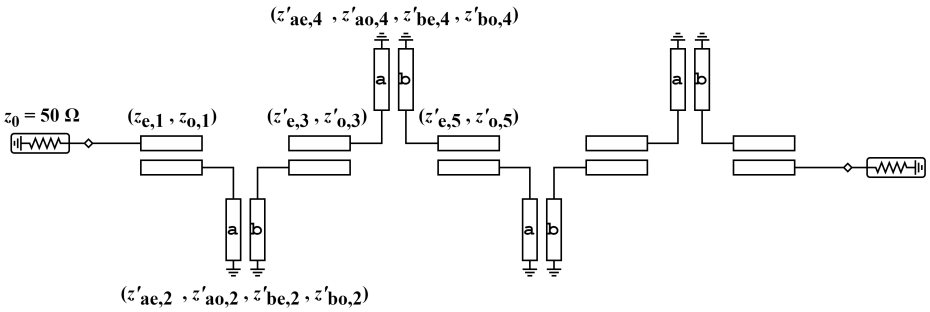

Schematic has odd symmetry.
Open-circuited coupled-line sections are $2\theta_c$ long at f_0.
Short-circuited coupled-line sections are θ_c long at f_0.

Δ	m	θ_c	$z_{e,1}$	$z_{o,1}$	$z'_{ae,2}$	$z'_{ao,2}$	$z'_{be,2}$	$z'_{bo,2}$	$z'_{e,3}$	$z'_{o,3}$	$z'_{ae,4}$	$z'_{ao,4}$	$z'_{be,4}$	$z'_{bo,4}$	$z'_{e,5}$	$z'_{o,5}$
0.05	5	30°	61.072	38.934	51.244	44.142	51.118	44.016	48.832	46.280	49.937	45.160	49.945	45.168	48.733	46.379
	6	25.714°	61.772	38.235	83.228	73.599	83.052	73.423	48.539	45.935	81.453	74.978	81.463	74.989	48.438	46.035
	7	22.5°	62.454	37.558	119.765	107.257	119.532	107.024	48.229	45.598	117.458	109.050	117.472	109.064	48.127	45.699
	8	20°	63.091	36.922	160.725	144.992	160.438	144.704	47.911	45.267	157.829	147.254	157.847	147.272	47.808	45.369
	9	18°	63.690	36.320	205.999	186.721	205.652	186.374	47.589	44.942	202.463	189.493	202.485	189.515	47.486	45.044
0.1	5	30°	65.284	34.725	52.650	39.100	52.153	38.602	47.773	42.908	49.864	40.756	49.889	40.782	47.585	43.095
	6	25.714°	66.234	33.792	84.000	65.721	83.318	65.038	47.231	42.295	80.237	67.966	80.273	68.002	47.041	42.486
	7	22.5°	67.091	32.930	119.427	95.843	118.530	94.947	46.664	41.708	114.563	98.724	114.616	98.777	46.472	41.899
	8	20°	67.897	32.117	158.741	129.284	157.613	128.156	46.088	41.139	152.674	132.874	152.740	132.941	45.897	41.330
	9	18°	68.669	31.346	201.797	165.884	200.416	164.503	45.512	40.587	194.401	170.263	194.481	170.344	45.322	40.778
0.15	5	30°	68.376	31.679	54.243	34.748	53.190	33.696	46.808	39.835	49.818	36.765	49.879	36.826	46.538	40.104
	6	25.714°	69.409	30.641	85.108	58.997	83.652	57.541	46.053	39.018	79.173	61.683	79.256	61.766	45.782	39.290
	7	22.5°	70.392	29.661	119.663	86.141	117.776	84.254	45.271	38.245	112.055	89.581	112.158	89.684	45.002	38.514
	8	20°	71.297	28.750	157.686	116.019	155.315	113.648	44.484	37.507	148.220	120.276	148.359	120.415	44.217	37.774
	9	18°	72.156	27.892	198.983	148.478	196.064	145.559	43.706	36.799	187.491	153.604	187.663	153.776	43.441	37.063
0.2	5	30°	70.738	29.316	55.924	30.992	54.090	29.158	45.925	37.024	49.711	33.032	49.808	33.129	45.590	37.361
	6	25.714°	71.873	28.188	86.402	53.161	83.911	50.671	44.987	36.052	78.127	55.885	78.263	56.021	44.651	36.389
	7	22.5°	72.968	27.123	120.280	77.778	117.058	74.556	44.023	35.143	109.688	81.270	109.861	81.444	43.689	35.478
	8	20°	73.945	26.150	157.205	104.660	153.199	100.653	43.062	34.285	144.121	108.956	144.351	109.186	42.732	34.617
	9	18°	74.859	25.245	197.039	133.594	192.186	128.742	42.120	33.472	181.259	138.812	181.534	139.087	41.792	33.801

dimensions by using multi-layer substrates as highlighted in Section III-B.

REFERENCES

[1] J. Chen, Y. Li, W. Qin, Y. Yang, and Z. Bao, "Compact multi-layer bandpass filter with wide stopband using selective feeding scheme," *IEEE Trans. Circuits Syst. II, Exp. Briefs*, vol. 65, no. 8, pp. 1009–1013, Aug. 2018.

[2] W. Feng, X. Ma, R. Gomez-Garcia, Y. Shi, W. Che, and Q. Xue, "Multi-functional balanced-to-unbalanced filtering power dividers with extended upper stopband," *IEEE Trans. Circuits Syst. II, Exp. Briefs*, vol. 66, no. 7, pp. 1154–1158, Jul. 2019.

[3] A. Sheikhi, A. Alipour, and A. Mir, "Design and fabrication of an ultra-wide stopband compact bandpass filter," *IEEE Trans. Circuits Syst. II, Exp. Briefs*, vol. 67, no. 2, pp. 265–269, Feb. 2020.

[4] D. Wu, Y. C. Li, Q. Xue, W. Feng, and B. Hu, "Synthesis and design of LTCC filtering balun with wide stopband," *IEEE Trans. Circuits Syst. II, Exp. Briefs*, vol. 67, no. 8, pp. 1404–1408, Aug. 2020.

[5] L. Qiu and L. Zhu, "Wideband filtering differential phase shifter with enhanced harmonic suppression," *IEEE Microw. Wireless Compon. Lett.*, vol. 31, no. 5, pp. 445–448, May 2021.

[6] D. Tang and X. Luo, "Compact filtering balun with wide stopband and low radiation loss using hybrid microstrip and substrate-integrated defected ground structure," *IEEE Microw. Wireless Compon. Lett.*, vol. 31, no. 6, pp. 549–552, Jun. 2021.

[7] Y. Xie and F. Chen, "Dual-band and wide stopband coaxial filters using open-circuited-stub-loaded resonators," *IEEE Trans. Circuits Syst. II, Exp. Briefs*, vol. 68, no. 6, pp. 1872–1876, Jun. 2021.

[8] L.-L. Qiu and L. Zhu, "Synthesis design of filtering differential phase shifters of independently suppressed harmonics," *IEEE Trans. Circuits Syst. II, Exp. Briefs*, vol. 68, no. 8, pp. 2760–2764, Aug. 2021.

[9] M. Ma, F. You, T. Qian, C. Shen, R. Qin, T. Wu, and S. He, "A wide stop-band dual-band bandpass filter based on asymmetrical parallel-coupled transmission line resonator," *IEEE Trans. Microw. Theory Techn.*, vol. 70, no. 6, pp. 3213–3223, Jun. 2022.

[10] W. M. Fathelbab and M. B. Steer, "Parallel-coupled line filters with enhanced stopband performances," *IEEE Trans. Microw. Theory Techn.*, vol. 53, no. 12, pp. 3774–3781, Dec. 2005.

[11] R. V. Snyder and S. Shin, "Parallel coupled line notch filter with wide spurious-free passbands," in *IEEE MTT-S Int. Microw. Symp. Dig.*, Jun. 2005, pp. 253–256.

[12] R. Levy, R. V. Snyder, and S. Shin, "Bandstop filters with extended upper passbands," *IEEE Trans. Microw. Theory Techn.*, vol. 54, no. 6, pp. 2503–2515, Jun. 2006.

[13] P. I. Richards, "Resistor-transmission-line circuits," *Proc. IRE*, vol. 36, no. 2, pp. 217–220, Feb. 1948.
[14] A. Podcameni and L. F. M. Conrado, "A new transmission-line identity," *Microw. Opt. Technol. Lett.*, vol. 23, no. 1, pp. 62–63, Oct. 1999.
[15] G. L. Matthaei, L. Young, and E. M. T. Jones, *Microwave Filters, Impedance-Matching Networks, and Coupling Structures*. Dedham, MA, USA: Artech House Books, 1980.
[16] H. Ozaki and J. Ishii, "Synthesis of a class of strip-line filters," *IRE Trans. Circuit Theory*, vol. 5, no. 2, pp. 104–109, 1958.
[17] R. J. Wenzel, "Exact design of TEM microwave networks using quarter-wave lines," *IEEE Trans. Microw. Theory Techn.*, vol. MTT-12, no. 1, pp. 94–111, Jan. 1964.
[18] G. I. Zysman and A. K. Johnson, "Coupled transmission line networks in an inhomogeneous dielectric medium," *IEEE Trans. Microw. Theory Techn.*, vol. MTT-17, no. 10, pp. 753–759, Oct. 1969.
[19] S.-M. Wang, C.-H. Chi, M.-Y. Hsieh, and C.-Y. Chang, "Miniaturized spurious passband suppression microstrip filter using meandered parallel coupled lines," *IEEE Trans. Microw. Theory Techn.*, vol. 53, no. 2, pp. 747–753, Feb. 2005.

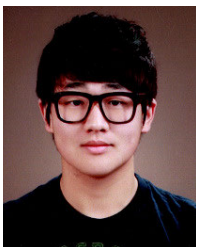

JONGHEUN LEE (Graduate Student Member, IEEE) received the B.E. degree in computer and communication engineering from Korea University, Seoul, South Korea, in 2019, where he is currently pursuing the Ph.D. degree in radio communications engineering.

His current research interest includes planar microwave circuits. He was a recipient of first prize in the Student and Young Engineer Design Competition from the 2022 Asia-Pacific Microwave Conference.

MINHYUP SONG (Member, IEEE) received the B.S. degree in electrical engineering from Korea University, Seoul, South Korea, in 2006, and the direct Ph.D. degree in electrical engineering from Purdue University, West Lafayette, IN, USA, in 2012. From 2009 to 2012, he was a Research Assistant with the Ultrafast Optics and Optical Fiber Communications Laboratory. He was engaged in research on microwave photonic filter design based on optical frequency comb source, where his research result was highlighted by Nature Photonics. In 2013, he joined the Components and Material Research Laboratory, Electronics and Telecommunication Research Institute (ETRI), as a Senior Researcher, where he is currently involved in optical frequency comb sources and line-by-line pulse shaping. He is a member of the Optical Society of America. He has served as a Reviewer for *Optics Letters*, *Optics Express*, *Applied Optics*, IEEE PHOTONIC TECHNOLOGY LETTERS, and *Journal of the Optical Society of America B*. He has also won awards, including IBC top 100 scientists, in 2016, and the Haedong Young Engineering Researcher Award by IEEE Korea, in 2020.

JUSEOP LEE (Senior Member, IEEE) received the B.Eng. and M.Eng. degrees in radio science and engineering from Korea University, Seoul, South Korea, in 1997 and 1999, respectively, and the Ph.D. degree in electrical engineering from the University of Michigan, Ann Arbor, MI, USA, in 2009.

In 2001, he joined the Electronics and Telecommunications Research Institute (ETRI), Daejeon, South Korea, where he was involved in the design of passive microwave equipment for Ku- and Ka-band communications satellites. In 2005, he joined the University of Michigan, where he was a Research Assistant and a Graduate Student Instructor with the Radiation Laboratory and was involved in research activities focused on millimeter-wave radars and synthesis techniques for multiple-passband microwave filters. In 2009, he joined Purdue University, West Lafayette, IN, USA, as a Postdoctoral Research Associate, where he was involved in the design of adaptable RF systems. In 2012, he joined Korea University, where he is currently a Professor. From 2019 to 2020, he was a Visiting Professor with the University of Virginia, Charlottesville, VA, USA. His current research interests include RF and microwave circuits, satellite transponders, and wireless power transfer systems.

Prof. Lee was a recipient of the Best Teaching Award presented by Korea University for Spring 2018 and Fall 2018. He was an Associate Editor of the IEEE TRANSACTIONS ON MICROWAVE THEORY AND TECHNIQUES, from 2017 to 2019.